Catalysis Letters Vol. 100, Nos. 3–4, April 2005 (© 2005)
DOI: 10.1007/s10562-004-3459-0

Effect of the particle size on the activity of MoO_xC_y catalysts for the isomerization of heptane

L.O. Alemán-Vázquez[a,b,*], E. Torres-García[a], J.R. Villagómez-Ibarra[b], and J. L. Cano-Domínguez[a]

[a]*Instituto Mexicano del Petróleo, Programa de Tratamiento de Crudo Maya, Eje Central Lázaro C á rdenas 152, Col. San Bartolo Atepehuacan, 07730 México, D.F., México*

[b]*Centro de Investigaciones Químicas, Universidad Autónoma del Estado de Hidalgo, Ciudad Universitaria, Carr. Pachuca-Tulancingo km 4.5, 042076 Pachuca, Hgo, México*

Received 19 July 2004; accepted 1 December 2004

Molybdenum trioxide samples having apparent particle sizes (APS) of 5 and 20 μ.m were partially reduced under flow of a mixture of H_2/*n*-heptane during 4 h. X-ray diffraction and Raman spectroscopy showed the typical structural transformation of MoO_3 into MoO_xC_y and MoO_2. These structural changes occur preferentially on the {0k0} planes. After the reduction treatment the resulting materials, having surface areas of 23 and 53 m^2/g, were evaluated in the isomerization of *n*-heptane at 643 K and 18.5 bar. The catalyst with an APS of 20 μ.m showed a maximum conversion around 70%, while for the catalyst with an APS of 5 μ.m the maximum conversion was 34%. The lower activity of the 5 μ.m MoO_xC_y catalyst seems to be related to a faster rate of formation of oxygen vacancies and rearrangement of the lattice into a more stable and less active structure in the case of small-size particles, due to a higher concentration of terminal Mo=O bonds along the *a*- and *b*-axes, which facilitate the electrophilic attack by hydrogen on the (010) plane.

KEY WORDS: molybdenum oxycarbide; heptanes isomerization; particle size; Raman spectroscopy; X-ray diffraction.

1. Introduction

In order to increase the octane number in gasolines, the refining industry uses some high-octane components that are paraffinic in nature, such as alkylate and isomerate. These components are constituted by highly branched isomers and have a relatively low environmental impact. Virgin naphtha is highly paraffinic, but commercial isomerization catalysts present high cracking rates when the feedstock contains C_7+ paraffins, and this fraction is usually processed in reforming units. The high aromatics content in reformate results in a high octane number but aromatics also have high photochemical activities. The interest of the refining industry in the production of clean fuels has led to the search for catalysts with improved activity and selectivity for the isomerization of C_7+ paraffins.

Compounds of groups V, VI and VII transition metals have been widely used as catalysts for the isomerization of different types of hydrocarbons. The carbides of tungsten and molybdenum are characterized by their high thermal stability and surface reactivity in heterogeneous catalysis. It has been shown that the oxidation of these carbides leads to an active and selective material for the isomerization of paraffins. For example, molybdenum carbide and oxycarbide have been used in the isomerization of hexanes and heptanes [1–3].

* To whom correspondence should be addressed.
E-mail: laleman@imp.mx

Molybdenum oxycarbide has been prepared by direct reduction of MoO_3 with a carbon-rich source at temperatures around 623 K [1–3]. During the reduction process different phases are formed, one of which is the molybdenum oxycarbide (MoO_xC_y) [4–7]. The reduction of MoO_3 is the crucial step in the formation of active catalysts for the isomerization of alkanes and has been widely studied. The composition and structure of the phases formed in this reduction process have been studied by X-ray diffraction, Raman spectroscopy and electron microscopy in order to understand the nature and evolution of the catalytically active phase [4–10].

The mechanism of alkanes isomerization has been discussed for a long time. The details of the mechanism are, however, still unresolved. The main problems to be solved include the mechanism of formation of carbenium ions, the effect of the acidity of the catalyst and the role of the metallic component.

The evolution of the surface area of molybdenum oxycarbide samples as a function of temperature and time on stream has been reported by Delporte *et al.* [5,6] and some information on the relationship between surface area and activity of this material for the isomerization of *n*-paraffins has been presented by Delporte *et al.* [6] and Ledoux *et al.* [8]. However, there is no information published on the effect of the particle size of MoO_3 on the activity of molybdenum oxycarbide as an isomerization catalyst. In this work we present the results of the isomerization of *n*-heptane using MoO_3 with two different particle sizes.

2. Experimental

2.1. Molybdenum oxycarbide preparation

Two different MoO_3 samples (1 g) having particle sizes of 5 and 20 μ.m were placed in a continuous flow stainless steel reactor (0.9 cm in diameter) and the temperature was raised to 643 K under hydrogen flow. The pressure was kept at 18.5 bar. Afterwards, *n*-heptane (99% purity) was fed to the reactor at a rate of 5 mL/h during 4 h using an LDC analytical minipump. The hydrogen flow was controlled using a Brooks 5850E mass flow controller to keep a H_2/nC_7 molar flow ratio of 39/1.

2.2. Isomerization reaction

After the molybdenum oxycarbide preparation, the corresponding heptane isomer (*n*-heptane, 3-methylhexane (98% purity) or 2,3-dimethylpentane (99% purity)) was fed to the reactor. Samples of the reaction product were collected at different times during the test and analyzed in an Agilent 6890 gas chromatograph with PIANO software.

2.3. Characterization

The surface areas of the samples were determined by the BET method using a Micromeritics ASAP system, and the particle size was determined by the ASTM D-4464-00 method (Standard Test Method for Particle Size Distribution of Catalytic Material by Laser Light Scattering).

The molybdenum oxide and oxycarbide samples were characterized by means of X-ray diffraction using a Siemens diffractometer (Model D5000) with Cu K_α radiation and a Ni filter. The operating conditions were 30 kV and 20 mA in the angular range 4–70° in 2θ. Crystalline phase identification based on XRD patterns was aided by the ICDD-PDF-2 database.

The Raman spectra of MoO_3 and MoO_xC_y at different times were obtained in air at room temperature with a double monochromator Raman spectrometer (SPEX Mod. 1403) using an Ar^+ ion laser which delivered 10 mW of incident radiation. The excitation line of the laser was 514.5 nm. The Raman signal was detected with a photomultiplier and a standard photon counting system.

Scanning electron microscopy (SEM) was carried out in an ESEM XL30 microscope equipped with an EDAX X-ray detector.

3. Results and discussion

3.1. Structural transformation of MoO_3 into MoO_xC_y

3.1.1. Surface area

The surface areas of the MoO_xC_y samples after 4 h of reduction treatment of MoO_3 with particle sizes of 5 and 20 μ.m were determined to be 23 and 53 m^2/g, respectively.

3.1.2. X-ray diffraction

XRD patterns of MoO_3 samples in both particle sizes are nearly identical. XRD patterns of samples of MoO_xC_y after reduction of MoO_3 in both sizes with a mixture of H_2/n-C_7 at 643 K are also very similar. Representative results are presented in Figure 1. For the starting material, narrow diffraction lines corresponding to MoO_3 were detected (JCPDS data file no. 35-609). The intensities of the {0k0} diffraction lines were remarkably high. This is due to the structure of MoO_3, which is formed by layers of [MoO_6] octahedrons, stacked along the [010] direction, which favors platelet crystallites with a preferential orientation along this axis. For the MoO_xC_y samples, the XRD patterns indicated the presence of two new phases besides MoO_3. These phases are unequivocally related to MoO_2 and "carbon-modified MoO_3" structures, the latter having interplanar distances *d* of 0.61798, 0.3059 and 0.2040 nm (Figure 1), which is in agreement with previous reports [6,7, 11].The carbon-modified MoO_3 can be interpreted from a structural point of view as the result of the contraction of the distances between the planes of MoO_6 octahedrons, bound together by Van der Waals interactions in the direction [010], motivated by the simultaneous reduction of MoO_3 and substitution of oxygen atoms with carbon atoms to form the MoO_xC_y. The XRD patterns suggest a planar structure of MoO_xC_y reminiscent of the MoO_3 planes. The XRD diagrams for the samples obtained after 10 and 30 h

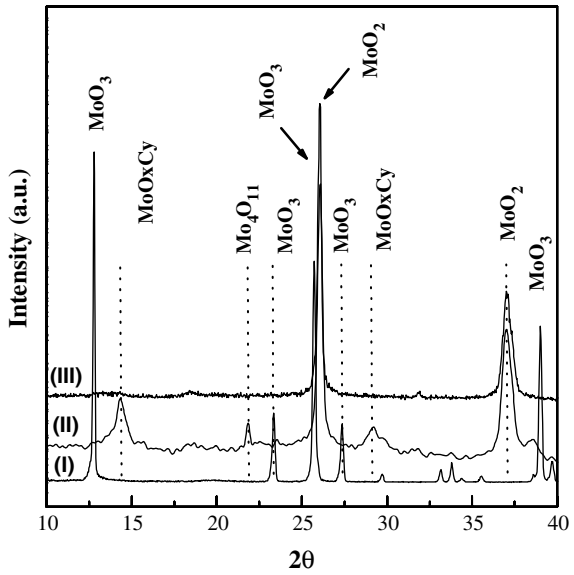

Figure 1. XRD patterns of the molybdenum oxide samples before and after treatment, (I) MoO_3 (orthorhombic system JC-PDF2-No. 05–0508), (II) MoO_xC_y obtained after 4 h of reduction treatment with a mixture of H_2/n-C_7 at 643 K, (III) MoO_2 (JCPDS data file no. 32-671) obtained after 10 h of reduction treatment.

under flow of the reductive mixture show the presence only of MoO_2 (JCPDS data file no. 32-671). Therefore, the formation of a critical concentration of oxygen vacancies on the (010), (100) and (001) planes during the reduction treatment promotes the collapse of the lattice and its reorganization into the MoO_2structure [5,6].

Additionally, in both cases, the well-know Mo_4O_{11} phase, which is an intermediate in the hydrogen reduction of MoO_3 [11], was detected.

3.1.3. Raman spectroscopy

There is no difference between the spectra of MoO_3 samples in both particle sizes, or between the spectra of samples of MoO_xC_y obtained by reduction of MoO_3 in both sizes. Characteristic Raman spectra of the structural behavior of MoO_3 and MoO_xC_y after 4, 6 and 10 h of reduction treatment are shown in Figure 2. Raman bands at 471, 666, 820 and 996 cm^{-1} correspond to orthorhombic MoO_3, while bands at 461, 495, 571, 589 and 744 cm^{-1} are characteristic of monoclinic MoO_2 obtained during the experiments, which is in agreement with our XRD results and previous work [12,13].

Furthermore, this same figure 2 shows the evolution of the Raman spectra at different reaction times of the reduction process of the MoO_3 phase and its conversion into MoO_2. The bands at 820 and 996 cm^{-1} significantly decreased in intensity and resolution with reaction time. Moreover, figure 2 indicates that the (MoO_xC_y) phase is highly disordered, which is in agreement with the XRD results (figure 1); this is due to the increase in oxygen defects and the incorporation of carbon atoms in the oxide matrix. This increase in the concentration of

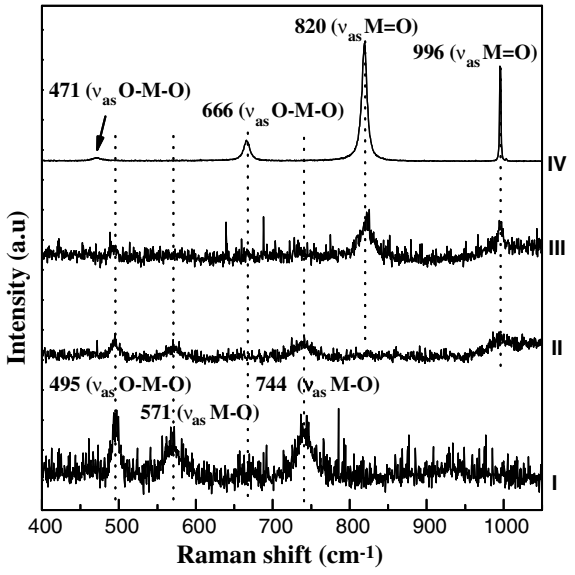

Figure 2. Characteristic Raman spectra of the molybdenum oxide samples before and after treatment: (I) typical spectra of MoO_2 after 10 h of reduction of MoO_3, (II) and (III) MoO_xC_y after 6 and 4 h of reaction under reductive mixture of H_2/n-C_7 at 643 K and IV) starting metal oxide (MoO_3).

oxygen vacancies and in the degree of substitution of oxygen by carbon atoms cause the rearrangement of the MoO_3 lattice, thus eliminating vacancies by local collapse and leading to the nucleation and growth of new phases. From this intermediate state and depending on the reduction process conditions, two products can be obtained, either MoO_2 or the MoO_xC_y phase [1,5,8].

After treatment of MoO_3 with the reductive mixture, the Raman bands at 996 and 820 cm^{-1} decreased in intensity until they completely disappeared, with the formation of a new band at 744 cm^{-1} attributed to the bridging of Mo–O vibrations in the MoO_2 [12,13] (Figure 2). These changes are associated with the degree of crystallinity of the samples and the lower oxygen/metal ratios.

The Mo = O bond distances along the *a*- and *b*-axes are shorter than the Mo–O bond distance along the *c*-axis. The Raman bands at 820 and 996 cm^{-1} can be assigned to the stretching vibration of the terminal Mo = O bonds along the *a*- and *b*-axes [12]. The bridging oxygen atoms (longer bond distances) along the *c*-axis are the most weakly bound, as shown by Mestl *et al.* [12,14]. This consideration suggests that the preferential generation of oxygen vacancies in the oxide matrix (MoO_3) can be along the *c*-axis, which is also indicated by the XRD results. Therefore, a displacement of the Mo atom toward the terminal oxygen in the *b*-direction can be expected upon the loss of the bridging oxygen, thus weakening the bond to the terminal oxygen atom along the *a*-axis.

Our results on the structural analysis of molybdenum oxycarbide using X-ray diffraction and Raman spectroscopy are in good agreement with previous reports [4,5,12,13,15,16]. However, it is not possible to conclude from these results which structural properties are related to the catalytic behavior of this material.

3.1.4. Scanning electron microscopy

In Figure 3 we can observe the morphology and the preferential growth of the particles along the (010) plane of the 5 μ.m (a) and 20 μ.m (b) MoO_3 samples. Figure 4 shows the molybdenum oxycarbide samples obtained after 12 h of reduction treatment of the 5 μ.m (a) and 20 μ.m (b) MoO_3. We can readily observe the appearance of defects on the surface of the samples. These defects appear to be generated by the reduction process and are present in a higher concentration in the 20 μ.m APS sample.

The accepted mechanism of reduction of MoO_3 [5,7,18,19,20] involves the adsorption and dissociation of hydrogen on the (010) plane and the elimination of water from two adjacent OH groups, forming oxygen vacancies randomly distributed on the surface. As the concentration of oxygen vacancies grows, there is a rearrangement and stabilization of the lattice by removal of point defects through the formation of crystallographic shear planes. The resulting molybde-

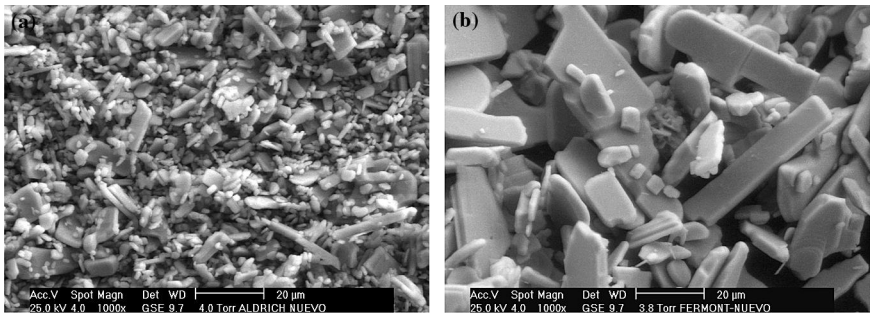

Figure 3. Scanning electron microscopy of the 5 μm (a) and 20 μm (b) MoO_3 samples.

num suboxide MoO_{3-x} may be described as a disordered shear structure in which the MoO_3 matrix is interrupted by irregularly spaced shear planes. As the reduction process proceeds, this rearrangement leads to the collapse of the MoO_3 orthorhombic layered structure into the monoclinic structure of MoO_2. The role of the carbon atoms in molybdenum oxycarbide seems to be related to the blockage of the shearing process by the stabilization of a metastable intermediate phase [7]. In the case of small-size particles, there is a higher concentration of terminal Mo = O bonds along the *a*- and *b*-axes, facilitating the electrophilic attack by hydrogen on the (010) plane and the formation and rearrangement of the oxygen vacancies. The lower concentration of defects observed in the sample obtained by reduction of the 5 μ.m APS MoO_3 could therefore be related to a faster rate of formation of oxygen vacancies and rearrangement of the lattice into a more stable structure.

3.2. Isomerization tests

3.2.1. Effect of the particle size on conversion

Tables 1 and 2 show the results of the isomerization of *n*-heptane with the MoO_xC_y catalysts obtained by reduction of the MoO_3 samples with 5 and 20 μ.m particle sizes.

The difference in the activity of the MoO_xC_y catalysts from MoO_3 with different particle sizes is remarkable. The catalyst prepared from MoO_3 with an APS of 20 μ.m showed a maximum conversion around 70%, while the maximum conversion for the catalyst prepared from MoO_3 with an APS of 5 μ.m was 34% (Figure 5). The selectivity to isomerization was slightly higher for the catalyst with an APS of 5 μ.m (98% vs. 96%).

A comparison of the activity of the 20 μ.m MoO_xC_y catalyst obtained in this work with the activity of a Pt/β zeolite catalyst reported by Ledoux *et al.* [1] is shown in table 3 and figure 6.

The activity of the 20 μ.m MoO_xC_y catalyst at 643 K is slightly lower than the activity of the Pt/β zeolite catalyst at 538 K. The most important differences between these catalysts are a higher selectivity to isomerization and a higher selectivity to dimethylpentanes for the MoO_xC_y catalyst.

3.2.2. Isomerization of branched paraffins

Additional tests were carried out using the MoO_xC_y catalyst with an APS of 20 μ.m, in order to evaluate the effect of the degree of branching of the feed paraffin on the conversion and selectivity to isomerization. Branched paraffins selected for this test were 3-methylhexane and 2,3-dimethylpentane, and the tests were carried out at the same conditions used for the isomerization of *n*-heptane. The results are shown in table 4 and figure 7.

For 3-methylhexane, the maximum conversion obtained was 56% and for 2,3-dimethylpentane it was 50%. Although these maximum conversions are lower than the one obtained for *n*-heptane (70%), they are still fairly high. The selectivity to isomerization was around 96% in both cases.

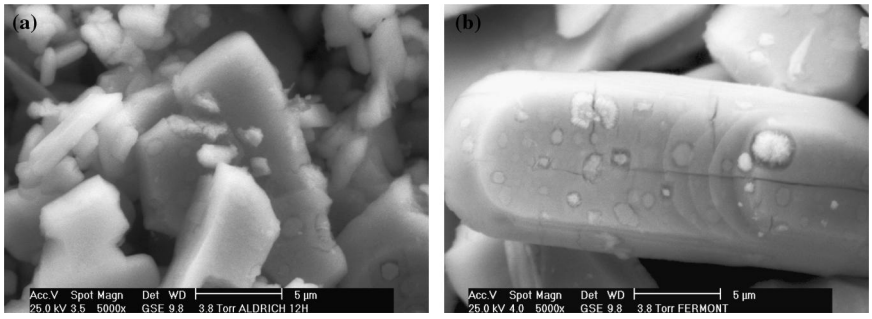

Figure 4. Scanning electron microscopy of the molybdenum oxycarbide samples obtained after 12 h of reduction treatment of the 5 μm (a) and 20 μm (b) MoO_3.

Table 1
Isomerization of *n*-heptane (643 K,18.5 bar) with MoO_xC_y catalysts (APS 5 μm)

Time on stream (h)	1	4	8	12	16	20	24	28	30
Composition weight (%)									
2,2-Dimethylpentane	0.154	0.361	0.656	0.558	0.588	0.553	0.623	0.542	0.533
2,4-Dimethylpentane	0.438	0.891	1.452	1.244	1.293	1.251	1.404	1.279	1.266
2,2,3-Trimethylbutane	0.017	0.034	0.062	0.050	0.053	0.052	0.061	0.057	0.057
3,3-Dimethylpentane	0.120	0.238	0.387	0.341	0.351	0.333	0.361	0.322	0.319
2-Methylhexane	5.056	9.637	13.096	12.638	12.937	12.654	13.238	12.512	12.446
2,3-Dimethylpentane	0.966	1.828	2.658	2.476	2.568	2.511	2.704	2.568	2.547
3-Methylhexane	5.464	10.521	14.341	14.059	14.391	14.042	14.529	13.677	13.595
3-Ethylpentane	0.417	0.791	1.0841	1.072	1.101	1.073	1.102	1.035	1.029
n-Heptane	86.828	75.000	65.241	66.546	65.819	63.638	64.931	66.904	67.157
Total (%)	99.485	99.469	99.378	99.231	99.380	96.358	99.310	99.242	99.248
Conversión (%)	12.549	24.462	34.291	32.977	33.709	35.709	34.603	32.616	32.361
Selectivity to isomerization (%)	100.939	99.827	98.925	98.904	99.277	90.923	98.865	98.620	98.774
Selectivity to cracking (%)	0.202	0.692	1.178	0.754	0.834	0.704	1.039	1.068	0.931

Table 2
Isomerization of *n*-heptane (643 K, 18.5 bar) with MoO_xC_y catalysts (APS 20 μm)

Time on stream (h)	1	4	8	12	20	24	28	30
Composition weight (%)								
2,2-Dimethylpentane	0.125	0.862	1.569	2.051	1.931	2.451	2.202	2.201
2,4-Dimethylpentane	0.454	2.063	3.000	3.540	3.327	3.748	3.585	3.662
2,2,3-Trimethylbutane	0.029	0.147	0.218	0.276	0.260	0.291	0.283	0.291
3,3-Dimethylpentane	0.096	0.614	1.044	1.330	1.292	1.574	1.425	1.399
2-Methylhexane	3.122	13.630	19.785	21.939	21.921	23.474	22.728	22.529
2,3-Dimethylpentane	0.834	3.740	5.549	6.405	6.374	6.969	6.719	6.645
3-Methylhexane	3.161	14.717	22.156	24.894	25.171	27.128	26.144	25.684
3-Ethylpentane	0.244	1.155	1.804	2.067	2.109	2.305	2.201	2.142
n-Heptane	91.353	60.837	42.399	34.132	34.825	29.243	31.598	32.235
Total (%)	99.508	99.018	98.831	98.899	98.816	98.940	98.780	98.740
Conversión (%)	7.992	38.727	57.297	65.623	64.925	70.547	68.175	67.534
Selectivity to isomerization (%)	100.945	95.896	96.803	95.842	96.691	96.916	96.369	96.190
Selectivity to cracking (%)	1.134	3.259	2.297	3.476	2.491	2.508	2.800	2.911

4. Conclusions

Molybdenum oxycarbide (MoO_xC_y) was obtained by reduction of two different samples of MoO_3 (5 and 20 μ.m apparent particle size) under flow of a H_2/*n*-heptane mixture at 643 K and 18.5 bar. The surface areas of the molybdenum oxycarbide samples after 4 h of reduction treatment were determined as 23 and 53 m^2/g, respectively.

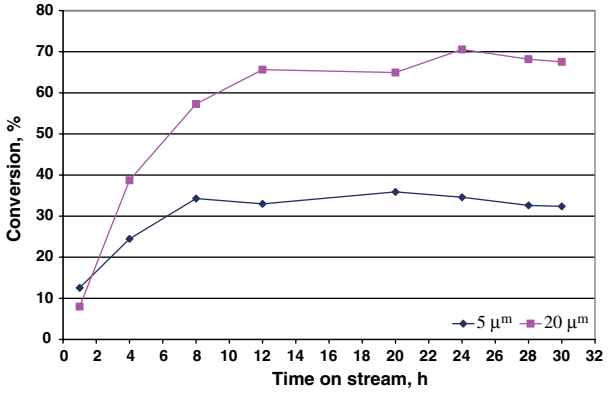

Figure 5. Effect of the apparent particle size of MoO_xC_y catalyst on conversion in the isomerization of *n*-heptane (643 K, 18.5 bar).

The XRD patterns of the molybdenum oxycarbide samples show the typical structural transformation of MoO_3 into MoO_xC_y and MoO_2. These structural changes occur preferentially on the {0k0} planes and specifically on terminal Mo=O bonds along the *a*- and *b*-axes. The XRD results correlate well with the changes in intensity and resolution of the Raman bands at 820 and 996 cm^{-1}, as the reduction time increases.

Scanning electron microscopy images of the molybdenum oxycarbide samples obtained after 12 h of reduction treatment of the 5 and 20 μ.m APS MoO_3 show the appearance of defects on the surface of the samples. These defects appear to be generated by the reduction process and are present in a higher concentration in the 20 μ.m APS sample.

Both molybdenum oxycarbide samples were tested in the isomerization of *n*-heptane at 643 K and 18.5 bar. A

Table 3
Comparison of results of the isomerization of *n*-heptane with the 20 μm MoO_xC_y catalyst and with a Pt/*β* zeolite catalyst [1]

Catalyst	0.8% Pt/*β* zeolite			MoO_xC_y		
Temperature (K)	538			643		
Pressure (bar)	15			18.5		
Time on stream (h)	1.0	4.0	24.0	4.0	12.0	24.0
Conversion (%)	22.7	23	22.2	38.7	65.5	70.5
Selectivity to isomerization (%)	88	88	90	96	96	97
Rate (10^{-6} mol g^{-1} s^{-1})	9.82	9.94	9.63	3.69	6.25	6.68
C_7 isomer distribution (%)						
Dimethyl pentanes	13.1	13.0	12.8	19.7	21.3	21.7
Methylhexanes	84.1	84.2	84.2	76.7	74.7	74.3
3 ethylpentane	2.3	2.3	2.4	3.1	3.3	3.3
Cyclic compounds	0.5	0.5	0.6	0.5	0.7	0.7
Cracked products (%)						
$C_6 + C_1$	3.6	3.4	3	28.9	35.14	51
$C_5 + C_2$	0.3	0.3	0.1	21.5	19.66	16.5
$C_4 + C_3$	91	91.3	92.8	49.6	45.19	32.5
Other	5.1	5	4.1	0	0	0

substantial difference in the activity of the MoO_xC_y catalysts with different particle sizes was found. The catalyst with an APS of 20 μ.m showed a maximum conversion around 70%, while the maximum conversion for the catalyst with an APS of 5 μ.m was 34%. The selectivity to isomerization was slightly higher for the 5 μ.m catalyst.

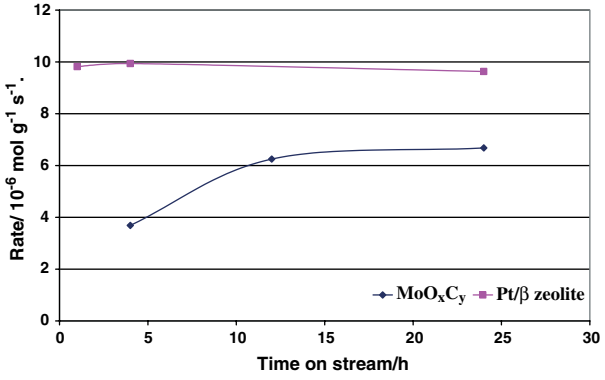

Figure 6. Catalytic activity of 20 μm MoO_xC_y al 643 K and Pt/β zeolite at 538 K in *n*-heptane isomerization.

The lower activity of the 5 μ.m MoO_xC_y catalyst seems to be related to a faster rate of formation of oxygen vacancies and rearrangement of the lattice into a more stable and less active structure in the case of small-size particles, due to a higher concentration of terminal Mo=O bonds along the *a*- and *b*-axes, which facilitate the electrophilic attack on the (010) planes by hydrogen.

Additional tests were carried out using the 20 μm MoO_xC_y catalyst with 3-methylhexane and 2,3-dimethylpentane as feedstocks. For 3-methylhexane, the maximum conversion obtained was 56% and for 2,3-dimethylpentane it was 50%. Although these maximum conversions are lower than the one obtained for *n*-hep-

Table 4
Isomerization of branched heptanes at 643 K with MoO_xC_y catalyst (APS 20 μm)

Feed	3-methylhexane			2,3-dimethylpentane			
Temperature (°C)	370	370	370	370	370	370	370
Time (h)	6	8	12	6	8	10	12
Composition (wt%)							
2,2-dimethylpentane	1.483	1.529	1.429	1.275	1.530	1.167	1.587
2,4-dimethylpentane	3.088	2.988	3.040	3.087	3.475	3.759	3.527
2,2,3-trimethylbutane	0.288	0.216	0.217	0.201	0.231	0.253	0.224
3,3-dimethylpentane	1.061	1.131	0.962	1.006	1.171	1.360	1.205
2-methylhexane	20.452	22.016	19.860	11.481	12.873	14.269	12.586
2,3-dimethylpentane	5.935	6.349	5.709	59.799	55.143	49.728	55.591
3-methylhexane	48.289	43.569	49.558	12.288	13.775	15.460	13.538
3-ethylpenane	1.947	2.228	1.857	1.002	1.123	1.269	1.108
n-heptane	15.751	18.573	15.145	8.260	9.150	10.584	9.093
Total	98.234	98.599	97.777	98.399	98.471	97.849	98.459
Conversion (%)	51.378	56.130	50.100	39.852	44.535	49.982	44.085
Selectivity to isomerization (%)	96.690	97.625	95.687	96.876	95.965	96.817	
Selectivity to cracking (%)	2.164	1.338	3.043	2.870	2.353	2.159	2.501

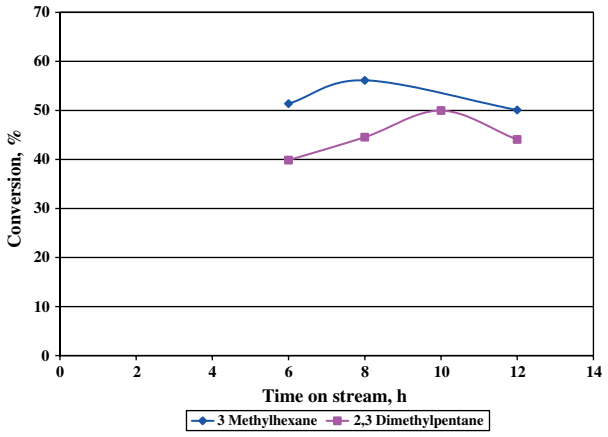

Figure 7 Conversion of 3-methylhexane and 2,3-dimethylpentane with MoO_xC_y catalyst (APS 20 μm).

tane (70%), they are still fairly high. The selectivity to isomerization was around 96% in both cases.

References

[1] M.J. Ledoux, P. Del Gallo, C. Pham-Huu and A.P.E. York, Catal. Today 27 (1996) 145.
[2] E.A. Blekkan, C. Pham-Huu, M.J. Ledoux and J. Guille, Ind. Eng. Chem. Res. 33 (1994) 1657.
[3] M.J. Ledoux, J. Guille, C. Pham-Huu, E.A. Blekkan and E. Peschiera, U.S. Patent (1996) 5 576,466.
[4] M.J. Ledoux, F. Meunier, B. Heinrich, C. Pham-Huu, M.E. Harlin and A.O.I. Krause, Appl. Catal. A 181 (1999) 157.
[5] P. Delporte, F. Meunier, C. Pham-Huu, P. Vennegues, M.J. Ledoux and J. Guille, Catal. Today 23 (1995) 251.
[6] P. Delporte, C. Pham-Huu and M.J. Ledoux, Appl. Catal. A 149 (1997) 151.
[7] C. Bouchy, C. Pham-Huu, B. Heinrich, C. Chaumont and M.J. Ledoux, J. Catal. 190 (2000) 92.
[8] M.J. Ledoux, C. Pham-Huu, P. Delporte, E.A. Blekkan A.P.E. York, E.G. Derouane and A. Fonseca, Sci. Tech. Catal. (1994) 81.
[9] A.P.E. York, C. Pham-Huu and P. Del Gallo, Catal. Today 35 (1997) 51.
[10] L.O. Alemán-Vázquez, E. Torres-García, G. Rodríguez-Gattorno, J. Ocotlán-Flores, M.A. Camacho- López and J.L. Cano, J. Solid State Chem. 177 (2004) 3281.
[11] T. Ressler, J. Wienold, R.E. Jentoft and T. Neisius, J. Catal. 210 (2002) 67.
[12] M. Dieterle, G. Weinberg and G. Mestl, Phys. Chem. Chem. Phys. 4 (2002) 812.
[13] M. Dieterle and G. Mestl, Phys. Chem. Chem. Phys. 4 (2002) 822.
[14] G. Mestl, N.F.D. Verbruggen, E. Bosch and H. Knözinger, Langmuir 12 (1996) 2961.
[15] J. Haber and E. Lalik, Catal. Today 33 (1997) 119.
[16] P. Wehrer, S. Libs and L. Hilaire, Appl. Catal. A 238 (2003) 69.
[17] Y. Ono, Catal. Today 81 (2003) 3.
[18] L.A. Bursill, Proc. Roy. Soc. A. 311 (1969) 267.
[19] P.A. Spevack and N.S. McIntyre, J. Phys. Chem. 97 (1993) 11020.
[20] P.A. Spevack and N.S. McIntyre, J. Phys. Chem. 97 (1993) 11031.